Available online at www.sciencedirect.com
ScienceDirect
Journal of the European Ceramic Society 29 (2009) 1347–1360
www.elsevier.com/locate/jeurceramsoc

Corrosion mechanism of polycrystalline corundum and calcium hexaluminate by calcium silicate slags

B.A. Vázquez [b], P. Pena [a,*], A.H. de Aza [a], M.A. Sainz [a], A. Caballero [a]

[a] *Instituto de Cerámica y Vidrio, C.S.I.C., C/Kelsen 5, Cantoblanco, 28049 Madrid, Spain*
[b] *Universidad Autónoma de Nuevo León–Monterrey, Nuevo León, Mexico*

Received 28 April 2008; received in revised form 22 August 2008; accepted 27 August 2008
Available online 19 October 2008

Abstract

The chemical reactions involved in the corrosion of polycrystalline alumina (Al_2O_3) and calcium hexaluminate–hibonite ($CaAl_{12}O_{19}$) ceramics by two dicalcium silicate slags with additions of fluorspar (CaF_2) were studied using a hot-stage microscopy (HSM) up to 1600 °C. The corrosion mechanism was investigated on *post-mortem* corroded samples and the phases formed at different stages of the dissolution process were characterised by reflected optical light microscopy (RLOM) and scanning electron microscopy (SEM) with energy dispersive X-ray spectrometry (EDS) microanalysis system.

The attack of the fused slags on dense alumina substrates takes place through an interdiffusion mechanism producing successive layers of calcium aluminates. In porous hibonite samples chemical interactions were observed although only a layer of calcium dialuminate was formed. A sintering process in presence of liquid phase was also detected behind the reaction interphase.

Thermodynamic calculations, based on the Al_2O_3–CaO–SiO_2, Al_2O_3–CaO–SiO_2–MgO, and Al_2O_3–CaO–SiO_2–CaF_2 phase equilibrium were used to further knowledge of the corrosion mechanism.

Keywords: Refractories; Corrosion; Alumina–dicalcium silicate slags; Calcium hexaluminate–dicalcium silicate slags

1. Introduction and literature review

Dissolution of refractory oxides in melt slags is of interest for understanding in-service refractory wear.[1–3] Chemical wear (corrosion) occurs as the system refractory/slag attempts to come to equilibrium when the slag is not saturated with a refractory component with it can dissolve. Thermodynamic equilibrium may only be achieved by the liquid dissolving enough of that refractory component to become saturated.

Extensive studies on dissolution of alumina, both as single crystal or dense polycrystalline Al_2O_3, in molten silicate slag have been the subject of many publications.[4–7]

Cooper,[8] Samaddar[9] and Oishi et al.[10] have performed analysis on both single crystals sapphire and polycrystalline Al_2O_3 corroded by a lime–aluminium-silicate slag at temperatures between 1525 °C and 1600 °C. These authors have determined the concentration distributions of CaO, Al_2O_3 and SiO_2 across liquid boundary layer and observed that a relative enrichment of the more mobile constituents of the slag occurred in the liquid boundary layer leading to formation of $CaAl_4O_7$ and $CaAl_{12}O_{19}$ as reactions products at the interface.

Sandhague and Yurek[11–13] in their studies on indirect dissolution of sapphire in calcia–magnesia–alumina-silicate melts, found that alumina-saturated melts containing 5 wt% of MgO forms mainly spinel at 1450 °C, while calcium hexaluminate is formed at 1550 °C. Higher contents of MgO in melts always produce $MgAl_2O_4$ at the interface under all conditions employed in their studies.

Guha[14] re-examined the dissolution of polycrystalline Al_2O_3 into a CaO–Al_2O_3–SiO_2 slag between 1400 °C and 1550 °C. This author detected two separated but interrelated reaction mechanism, one occurring on the Al_2O_3 surface and the other in the grain boundary of alumina. At the initial stages, a liquid boundary layer saturated with gehlenite, $Ca_2Al_2SiO_7$, was formed adjacent to the alumina surface. Later, the interaction between alumina and the different components present in the

* Corresponding author.
E-mail address: ppena@icv.csic.es (P. Pena).

0955-2219/$ – see front matter © 2008 Elsevier Ltd. All rights reserved.
doi:10.1016/j.jeurceramsoc.2008.08.031

liquid boundary produced the formation of a $CaAl_4O_7$ interface. However, with increasing temperature and time $CaAl_4O_7$ reacts with Al_2O_3 to form calcium hexaluminate, $CaAl_{12}O_{19}$, at the interface. On the grain boundary, the liquid became progressively enriched with alumina with a corresponding change in its composition. Finally, as the liquid is saturated in alumina, anorthite crystallized from the melt, and considering that anorthite is compatible with both, $CaAl_{12}O_{19}$ and Al_2O_3, no further reactions occurred and dissolution stopped at the bulk of the specimen.

Bates[15] also studied the corrosion of polycrystalline alumina and found that a slag containing 10/20 wt% of magnesia forms an $MgAl_2O_4$ spinel layer at the Al_2O_3/slag interface at 1502 °C. Bates identified gehlenite, $Ca_2Al_2SiO_7$, as a major reaction product near the interface at temperatures below 1427 °C. However, above this temperature, a second reaction product, identified as calcium hexaluminate, $CaAl_{12}O_{19}$, was found at the interface between gehlenite and alumina.

Shoichirou et al.[16] studied the kinetic behaviour of dissolution of sintered alumina in $CaO–SiO_2–Al_2O_3$ slags. The slags used had 10% Al_2O_3 and CaO/SiO_2 ratios from 0.64 to 1.25. They found that dissolution of alumina increased with increasing temperature and the dissolution rate was controlled by mass transport in the slag boundary layer. They also concluded that dissolution of alumina increased with increasing CaO/SiO_2 ratio and a sharp increase was observed in the vicinity of $CaO/SiO_2 = 1$.

Recently Zhang et al.[17] studied the dissolution of commercial white fused and tabular alumina grains into a model silicate slag at 1450 °C and 1600 °C. These authors observed the formation of calcium hexaluminate, $CaAl_{12}O_{19}$, and a hercynite spinel layer, $FeAl_2O_4$, at all alumina/slag interfaces. The hercynite spinel layer was not always continuous, and as compared with the $CaAl_{12}O_{19}$ layer hence had a less-significant effect on the dissolution process. The $CaAl_{12}O_{19}$ layer on the alumina was also incomplete in porous corundum grains. In both cases, slag penetration took place into the porous alumina grains.

As far as we are aware, no other work about corrosion behaviour or dissolution of calcium hexaluminate in melts constituted by alumina and/or calcium and/or silicate and/or magnesia had been reported in the literature.

The study described herein is focused to reveal details of the reaction behaviour of the alumina and calcium hexaluminate, two important phases present in many iron-making and steelmaking refractories, against calcium silicate steel slags. Microstructural characteristics of the reaction interface between both materials and slags were deeply studied by reflected light optical microscopy (RLOM) and scanning electron microscopy (SEM) with energy dispersive microanalysis (EDS) on different samples. Two typical calcium-based silicate steel slags (F and G), which contain ≈5 wt% of MgO and different amounts of Ca_2F (10 and 15 wt%), were chosen to develop the work.

The conditions, under which different phases are formed at the interface and in the bulk, of both specimens were also discussed taking into account the available phase equilibrium data[18] specifically those supplied by the following systems: $Al_2O_3–CaO–SiO_2$,[19] $Al_2O_3–CaO–SiO_2–MgO$[20–22] and $Al_2O_3–CaO/SiO_2/MgO–CaF_2$.[23–28]

2. Experimental procedures

2.1. Substrate synthesis

Calcium hexaluminate (hibonite, $CaAl_{12}O_{19}$) was prepared from a high purity $CaCO_3$ powder >99.5 wt% purity, with an average grain size of 13.8 μm and a specific surface of 0.2 $m^2\ g^{-1}$ from Merck (Darmstad, Germany), and high purity Al_2O_3 CT 3000SG powder >99.6 purity, with an average grain size 0.4 μm and specific surface 8 $m^2\ g^{-1}$ from Alcoa (Pittsburg, PA, USA). As a preliminary step, stoichiometric proportions of calcite and alumina were weighed ($CaO:6Al_2O_3$); next, to obtain a homogeneous and highly energetic milled batch, the mixtures were ground in a laboratory-scale attrition mill, with PSZ zirconia balls, in isopropanol media. After the milling process, the mixture was dried at 60 °C and burned at 950 °C for 2 h to remove CO_2. Then this powder was isostatically pressed to green compacts (200 MPa). This samples were heat treated at 1700 °C for 6 h at a heating and cooling rate of 5 °C min^{-1}. The reaction sintering temperature was selected taking into account the information provided by the $Al_2O_3–CaO$ system as evaluated and reported by Hallstedt.[29] The obtained material was ground in a tungsten carbide ball mill and then isostatically pressed and reheated again. This procedure was repeated once to obtain an X-ray diffraction pattern (Kristalloflex D5000, Siemens Germany), that showed the presence of hibonite as the only phase present (76-00665 card ASTM).

The bulk density of the obtained $CaAl_{12}O_{19}$ specimens, measured by the Archimedes method, was 86.5% of the theoretical value. The average grain size was ≈100 μm. Additional details of the specimens are given in Table 1.

Polycrystalline corundum (Al_2O_3) substrates were prepared by using high purity alumina powders (Alcoa CT 3000 SG). Dense compacts were obtained by heating at 1600 °C for 2 h isostatically pressed compacts (200 MPa). Additional details of these specimens are also given in Table 1.

Cylindrical plate specimens, 15 mm diameter and 4 mm thick were prepared from the two materials by cutting with a diamond

Table 1
Physical and chemical characteristics of the ceramic substrates.

	Ceramic materials	
	Al_2O_3	$CaAl_{12}O_{19}$
Chemical analysis (wt%)		
Al_2O_3	99.6	93.7
MgO	0.09	0.07
CaO	0.06	6.10
SiO_2	0.07	0.05
Na_2O	0.09	0.08
TiO_2	<0.01	<0.01
Mineralogical analysis	Corundum	Hibonite
Density (ρ/ρ_t, %)	98.0	86.5

Chemical analyses made by ICP.

Table 2
Chemical analyses of the slag (X-ray fluorescence).

	Ca_2SiO_4-based slags	
	F-slag	G-slag
Chemical analysis (wt%)		
Al	1.90	1.68
Mg	4.85	5.16
Ca	62.53	63.37
Si	28.26	22.47
Na	0.02	0
K	0	0
Cr	0.42	0.1
Fe	0.39	0.21
Ti	0.16	0.13
Mn	0.07	0.08
F	4.91	7.84
S	0.38	0.78
P	0.01	0.01
CaO/SiO_2 mol index	2.22	2.82

blade. The corresponding surface were subsequently polished to a mirror finish using 6, 3 and 1 μm diamond suspension and then cleaned in an ultrasonic bath.

Table 2 shows the composition of the slags used in this study. Both slags present as major constituents calcium oxide and silica, in proportion close to the Ca_2SiO_4 or Ca_3SiO_5. Other components are magnesium oxide ≈5 wt% and calcium fluoride, used as a flux additive, ≈10 wt% in the case of ferritic slag (F) and ≈15 wt% in the case of austenitic slag (G). Corrosion tests were performed at 1600 °C since this temperature corresponds to the usual slag's work conditions.

2.2. Corrosion diffusion couple pair system

In order to measure the corrosion of corundum and calcium hexaluminate substrates by both slags the reaction test method was used.[30] For the corrosion test, cylindrical specimens (1.5 mm diameter × 1.5 mm thickness) of the slag were used. These small and low compacted cylinders were placed in contact with the polished surfaces of both ceramic materials selected in this study. Any chemical reaction between the refractory and the partially/fully melted solid (slag) might lead to a reactant contact, which enables the reaction to take place resulting in transport of product matter that allows the corrosion chemical reaction to proceed.

The couple diffusion systems were fired up to 1600 °C at a constant heating rate of 5 °C/min. The experiment was performed inside a hot-stage microscopy (HSM) EM 201 equipped with an image analysis system and an electrical furnace 1750/15 (Leica, Germany). The temperature measurements were conducted in the vicinity of the specimens with a Pt3%Rh–Pt/Pt10%Rh thermocouple, which was place in contact with the ceramic plate used as support. The microscope projects the image of the sample through a transparent quartz window and the images were taken by a recording device. The computerized image analysis system automatically records and analyses the geometrical changes of the sample during heating. From images, the HSM software calculates geometrical variations, such as height, width and area of the sample and also contact angle between sample and substrate.

After firing, the specimens were mounted in an epoxy resin, and then cut perpendicular to the slag–ceramic interface. The cross section of each specimen was polished using 6, 3 and 1 μm diamond suspensions as an abrasive. Analysis of the crystalline phases were performed using reflected light optical microscopy and scanning electron microscopy with energy dispersive X-ray spectroscopy (Model DSM 950 Karl Zeiss, Thornwood, NY; Tracor Northern, Middleton, WI).

Microchemical analysis of the new layers formed at the reaction interface, was carried out by SEM/EDS on samples heat treated at 1570 °C or 1500 °C for a reaction time of 1 min. Compositional semi-quantitative microanalysis using the ZAF (atomic number absorption fluorescence) of SiO_2, CaO, Al_2O_3, MgO, TiO_2 and iron oxide were conducted across the slag–ceramic interface. Counting times were 60 s.

In addition, grain size measurements of the different crystalline phases were carried out by using the linear interception method on representative SEM micrographs.

3. Results and discussion

Both slags, treated at 1600 °C for 2 h, showed larnite (calcium disilicate, Ca_2SiO_4) as main component and consequently dusting effect during cooling was observed. This fact made it impossible to determine the microstructural characteristics of both slags by SEM.

3.1. Couple diffusion experimental studies

The reaction patterns for both ceramic/slag diffusion couple specimens were studied by a series of evaluations conducted on the slag. Contact angle and unreacted area of the substrate were also considered. In each case the observations was carried out *in situ*, during heat treatment inside the hot-stage microscopy, as explained in the experimental section. From these data, the reaction temperatures at the interface on the couple ceramic (alumina or hibonite)/slag F or G were established. The differences in the chemical composition of the substrates and slags produce different types of chemical reactions at the ceramic/slag interfaces.

The variation in slag area, calculated as a product of the height by the width of the slag compact, as a function of the temperature and substrate are shown in Figs. 1a and 2a. Photomicrographs of the sample shape evolution corresponding to each sample are shown in Figs. 1b and 2b. In these figures the typical changes in shape of the specimens (same heating schedule), can be seen. These figures also summarize the temperature values at which the initial and the maximum shrinkage of both slags were observed (1000 ± 5 °C and 1050 ± 5 °C, respectively). These temperatures are in good agreement with the temperatures of first liquid formation obtained from the corresponding phase equilibrium diagrams,[22–26] specifically the Ca_2SiO_4–CaF_2 pseudobinary system.

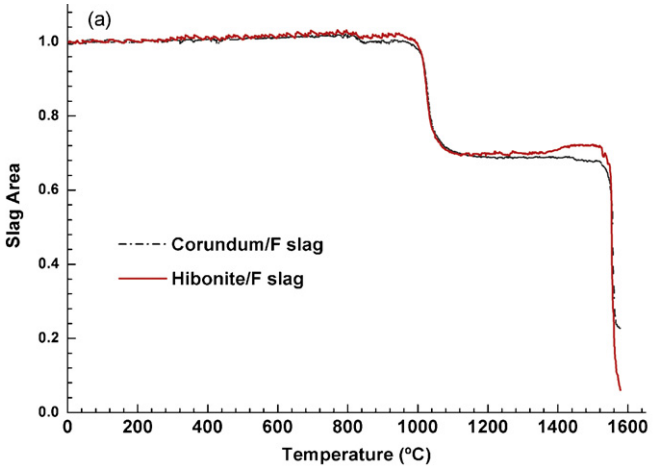

(b)	Room Temperature	Initial Shrinkage of slag	Maximum Shrinkage of slag	Reaction temperature	Flow
Corundum (Al_2O_3)/F-slag	25ºC	1000±5ºC	1050±5ºC	1555±5ºC	1560±5ºC
Hibonite ($CaAl_{12}O_{19}$)/ F-slag	25ºC	1000±5ºC	1050±5ºC	1555±5ºC	1560±5ºC

Fig. 1. (a) Variation in area of ceramic/F-slag samples during hot-stage microscopy (HSM) measurements (heating rate 5 °C min^{-1}). Test carried out at maximum temperature of 1578 °C. (b) Series of photomicrographs showing silhouettes corresponding to the high temperature typical behaviour pattern of the ceramic/F-slag couple diffusion samples.

At 1560 °C ± 5 °C simultaneous reaction and complete fusion of the slag proceeded at the alumina/F-slag interface of the coupling pair. The behaviour of the hibonite/F-slag interface was totally similar, a detectable chemical reaction and complete fusion took place at the same temperature. In the case of the G-slag (Fig. 2), the temperatures of chemical reaction at the interface were 1430 °C ± 5 °C and 1410 °C ± 5 °C for corundum and hibonite, respectively. The temperatures of complete fusion were also slightly different, 1475 °C ± 5 °C for alumina and 1450 °C ± 5 °C for hibonite.

The differences found in the temperature of reaction and/or temperature of complete fusion are consequence of the higher fluorspar content of G-slag, which reduced the viscosity of the melt increasing its reactivity and reducing the temperature of chemical reaction between slag and substrates.

It is well established[14] that CaF_2 is generally added to the calcium silicate melts in order to improve their fluidity. Recently Park and Min[31] studied the role of fluorspar and alumina in the viscous flow of the silicate melts (MgO = 10 wt%) at 1600 °C showing that viscosity of the basic melt decrease with increasing CaF_2 content up to about 15 wt%. These same authors also claimed that the viscosity of the basic melts also decreases by increasing the content of alumina up to 5 wt%. At higher values of alumina a slight increases takes place. The viscosity decrease up to 5 wt% Al_2O_3 is justified by the dissolution of larnite into the liquid phase, while the increase in the viscosity of the homogeneous liquid phase at higher Al_2O_3 wt% content is due to the increase in the degree of polymerization of the silicate network by the substitution of [SiO_4] tetraedra by [AlO_4] tetrahedra and [AlO_6] octahedral into the glass structure.

The results obtained in the present studies are in good agreement with Park's conclusions since the characteristics of the studied slags correspond with his deductions: (a) The G-slag contains more fluorspar and less larnite than the F-slag. (b) The differences in minor impurities and magnesium oxide content were unimportant concerning their high temperature behaviour. Consequently, the G-slag showed a higher reactivity than the F-slag against both substrates, although both substrates showed a similar behaviour against each type of slag.

3.2. Microstructural study by reflected optical light microscopy

Reflected light optical microscopy studies put in evidence that in all samples, slag–substrate reactions and saturation or near saturation state takes place, at high temperature, at time interval as short as 1 min. Fig. 3 shows typical microphotographs of the cross sections of polished samples, sketches with the texture of corroded samples can be also observed. After only 1 min of reaction at 1578 °C a complete chemical reaction took place

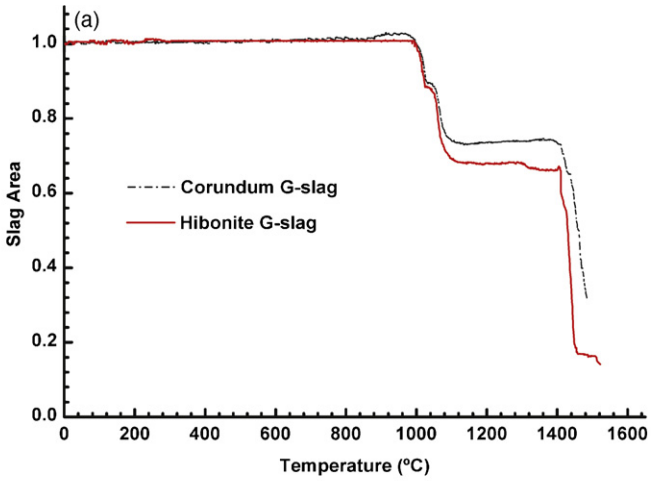

(b)	Room Temperature	Initial Shrinkage of slag	Maximum Shrinkage of slag	Reaction temperature	Flow
Corundum (Al_2O_3)/ G-slag	25ºC		1050±5ºC	1430±5ºC	1475±5ºC
Hibonite ($CaAl_{12}O_{19}$)/ G-slag	25ºC	1000±5ºC	1050±5ºC	1410±5ºC	1450±5ºC

Fig. 2. (a) Variation in area of ceramic/G-slag samples during hot-stage microscopy (HSM) measurements (heating rate 5 °C min^{-1}). Test carried out at maximum temperature of 1470 °C. (b) Series of photomicrographs showing silhouettes corresponding to the high temperature typical behaviour pattern of the ceramic/G-slag couple diffusion samples.

between alumina and hibonite substrates and F-slag (Fig. 3a and b). This strong interaction could be observed by naked-eye observations of couple diffusion systems (see sketches in Fig. 3c and d). The thicknesses of the interaction area were 500 μm for corundum and 300 μm for hibonite against F-slag and 600 μm for corundum and 400 μm for hibonite against G-slag (Figs. 4 and 6).

Fig. 3 also shows the formation of a double reaction layer at the substrate–slag interface in the case of alumina (Fig. 3a) and a single reaction layer in the case of hibonite (Fig. 3b). Alumina showed and homogeneous reaction front, while the most important feature of hibonite substrate was an irregular and inhomogeneous reaction front. Slag penetration was also observed in some areas of the hibonite substrate (Fig. 3b). The crystal habit of hibonite[32] produce less densification during sintering and consequently a more open microstructure as compared with alumina, which facilities the penetration of the slag into the substrate, through porosity and grain boundaries. The behaviour of substrates against G-slag was totally similar.

Finally, the RLOM study put in evidence that in the corundum/F-slag and corundum/G-slag samples, gehlenite was the main crystalline phase found in the slag while calcium dialuminate and calcium hexaluminate were generated, in this order, at the interface. Some crystals of magnesia–alumina spinel were also found in the slag region of the corundum/F-slag sample.

In the pairs calcium hexaluminate/F-slag and calcium hexaluminate/G-slag, only a layer of calcium dialuminate was found at the interface. This phase also crystallized in the slag.

3.3. Microstructural study by SEM and EDS microanalysis determinations

3.3.1. Alumina substrate

SEM micrographs of corundum/F-slag and corundum/G-slag specimens treated at 1578 °C and 1470 °C, respectively, are shown in Fig. 4a and b. The microstructures revealed two well-defined successive layers at the interface and no slag penetration into the alumina substrates. A massive formation of crystalline phases was observed in the slag face of the sample.

Changes in the concentration profile observed along the corundum/F-slag or corundum/G-slag interface (Fig. 5) indicates that calcium and silicon diffuses from the interface to the substrate even at a distance of 560 μm. A contradiffusion of aluminium from the substrate to the interface was observed.

At high magnification Fig. 6a and b reveal that at the interface there were two layers of reaction products (B and C) and a new phase crystallized in the slag (A) (Table 3).

In the A area (≈350 μm thick) of the corundum/F-slag sample (Fig. 6a), energy dispersive X-ray average analysis of the crystal-

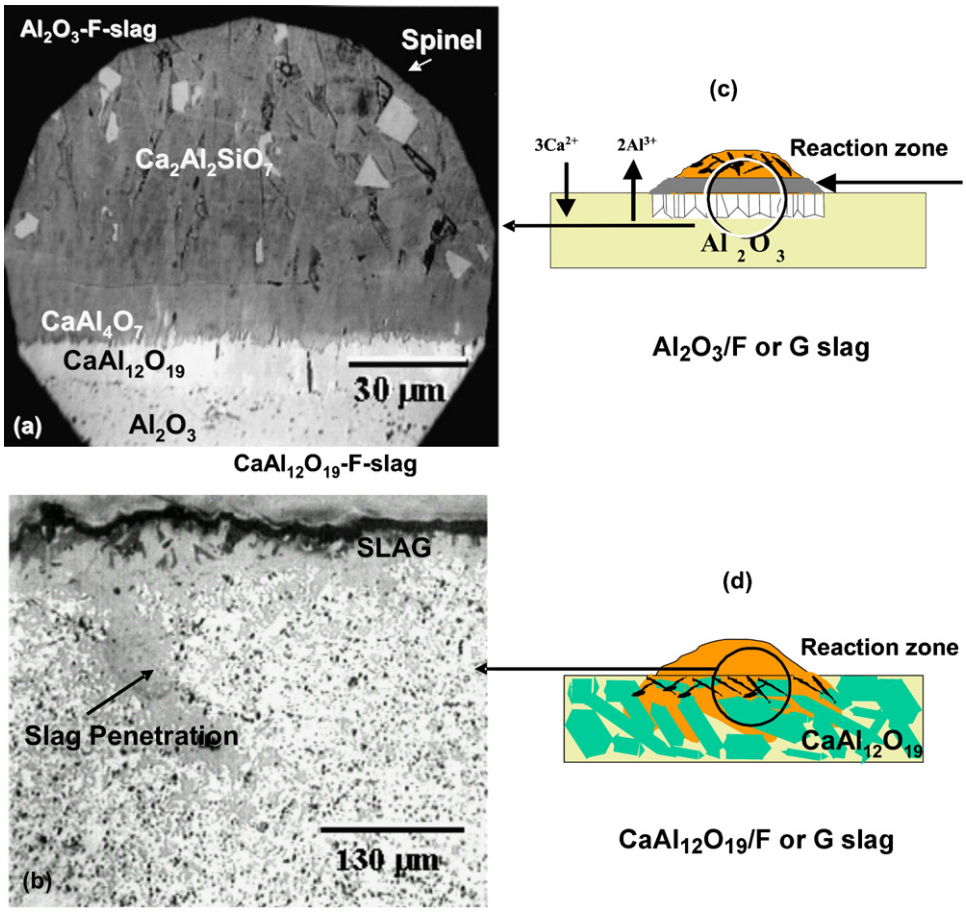

Fig. 3. Typical reflected light optical microphotographs of the cross sections of samples treated at 1578 °C. (a) Corundum/F-slag; (b) hibonite/F-slag; (c) sketch showing typical images of cross sections corundum/F or G-slag corroded samples; (d) sketch showing typical images of cross sections hibonite/F or G-slag corroded samples.

lized phase shows a composition close to gehlenite $Ca_2Al_2SiO_7$; (39.5 wt% CaO, 34.3 wt% Al_2O_3, 20.8 wt% SiO_2, 2.6 wt% MgO and 3.4 wt% of XO; XO = Fe, Ti, Cr).

This region contains as main crystalline phase light-grey elongated gehlenite$_{s.s}$ crystals with a punctual EDS microanalysis of 42.8 wt% CaO, 32.2 wt% Al_2O_3, 22.3 wt% SiO_2, 0.5 wt% MgO and 2.3 wt% of XO; XO = Fe, Ti, Cr. In this region, few isolated grey angular crystals of a complex spinel $[Mg, Fe, Ti]^{IV}$ $[Al, Fe, Ti, Cr]^{VI}$ O_4 with a composition 70.4 wt% Al_2O_3, 20.4 wt% MgO, 0.4 wt% CaO and 7.4 wt% of XO; XO = Fe, Ti, Cr, were also found. Small amount of elongated grey crystals of $CaAl_4O_7$ contained in the glassy phase were also observed.

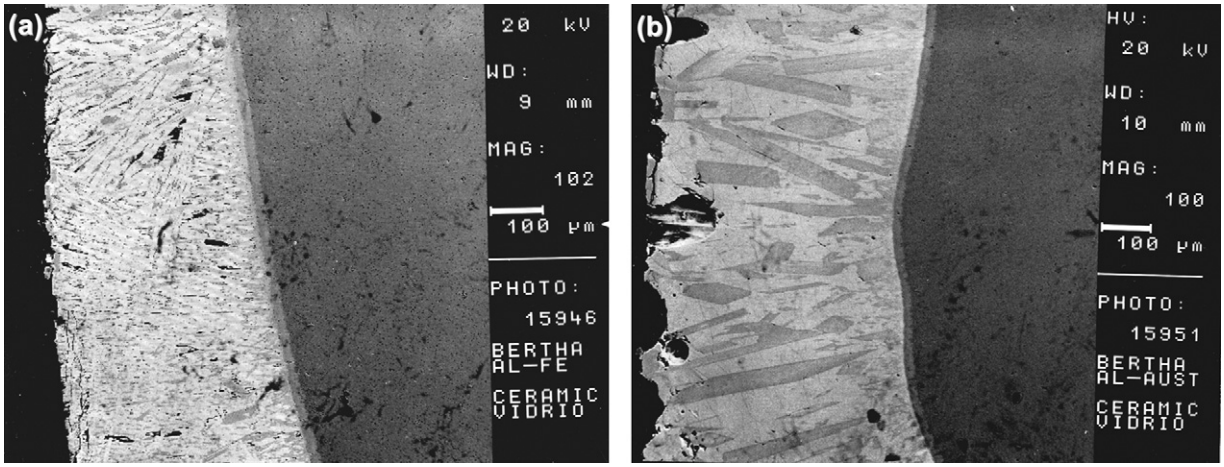

Fig. 4. (a) General SEM observations of the cross section of the Al_2O_3/F-slag sample fired at 1578 °C for 1 min. (b) General SEM view of the cross section of the Al_2O_3/G-slag sample fired at 1470 °C for 1 min.

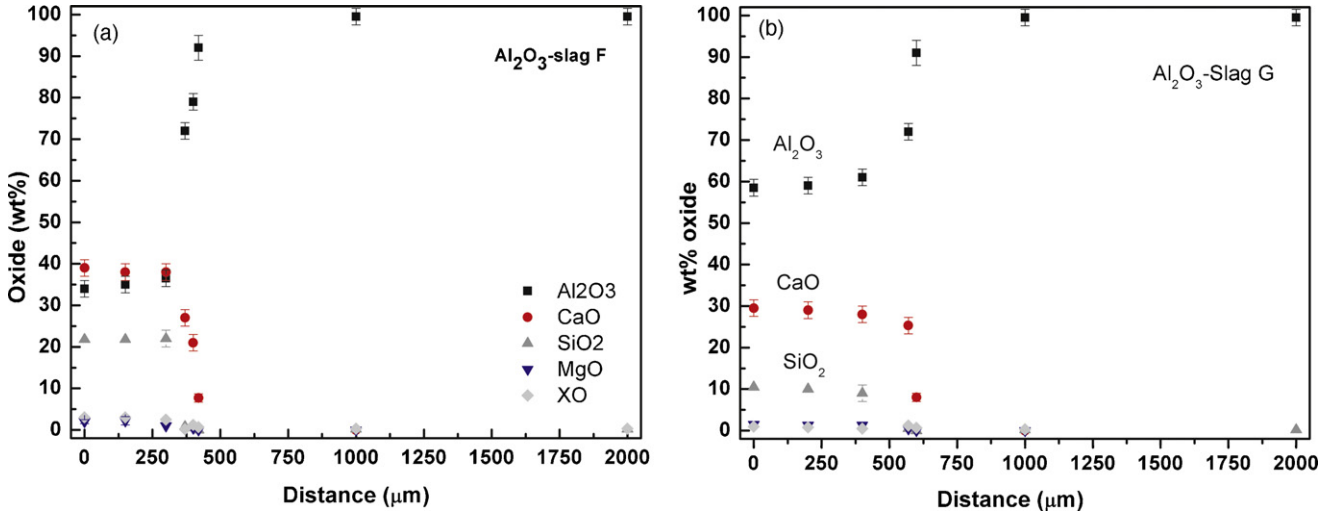

Fig. 5. Compositional profiles (20 μm × 50 μm) of reacted zone for (a) Al_2O_3/F-slag interface (maximum heating temperature 1578 °C) and (b) Al_2O_3/G-slag interface (maximum heating temperature 1470 °C).

At the interface (B region in Fig. 6a) a continuous thin-layer (≈7 μm width) formed by grey elongated crystals of $CaAl_4O_7$ (79.8 wt% Al_2O_3, 20.2 wt% CaO), with small amounts of a glassy phase at the grain boundary was remarked.

Another continuous layer (C region in Fig. 6a; ≈15 μm width) composed by grey and lath-like crystals of $CaAl_{12}O_{19}$ (SEM–EDS analysis: 93.9 wt% Al_2O_3, 6.1 wt% CaO) was observed. No liquid phase at grain boundaries was observed by SEM in this layer. Grain boundary microcracks propagating through the $CaAl_{12}O_{19}$ layer along the easy cleaved basal planes perpendicular to the $CaAl_{12}O_{19}$–Al_2O_3 interface are visible.[33,34] Although a line of small pores can be observed.

Finally the interfaces between alumina and calcium hexaluminate crystals (C/D boundary region in Fig. 6a), appeared well-bonded without evidence of cracks between Al_2O_3 and $CaAl_{12}O_{19}$. Although laths of $CaAl_{12}O_{19}$ often occurred in parallel groups, no obvious orientation relation existed between the $CaAl_{12}O_{19}$ crystals. Similar microstructures were observed in $CaCO_3$–corundum and $CaMg(CO_3)_2$–corundum reactive coatings pairs previously studied by Moya et al.[33] and De Aza et al.[34] Dense alumina substrate (D in the micrograph of Fig. 6), with an SEM–EDS microanalysis of 98.9 wt% Al_2O_3, 0.3 wt% CaO and 0.7 wt% SiO_2 was observed.

For the corundum/G-slag specimen (Fig. 6b) the microstructural features and thicknesses of resulting attack area were similar to the ones observed in corundum/F-slag sample (Fig. 6a). The more significant differences were found in the first reaction layer ($A \approx 560$ μm). This layer was only constituted by glassy phase and large gehlenite crystals. The composition of the glassy phase determined by energy dispersive X-ray average analysis (100 μm^2) was 28.8 wt% CaO, 61.3 wt% Al_2O_3, 9.4 wt% SiO_2, 1.3 wt% MgO and 0.5 wt% of XO; XO = Fe, Ti, Cr, while the composition of large ghelenite solid solution crystals were totally similar to that determined in the A-zone of

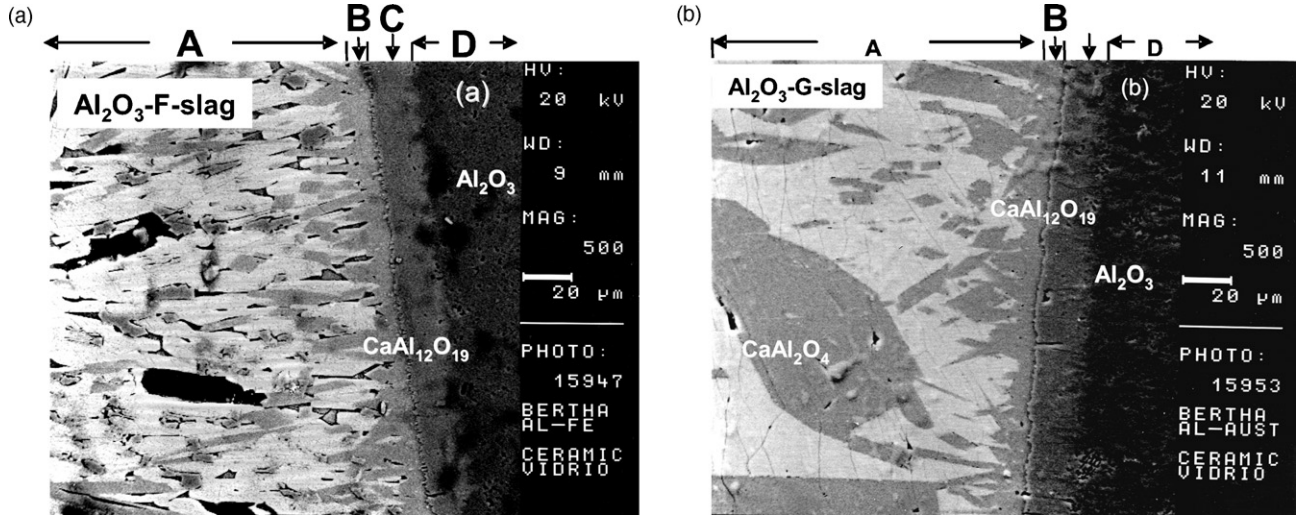

Fig. 6. Higher magnification SEM of: (a) the Al_2O_3/F-slag interface; (b) the Al_2O_3/G-slag interface. Both micrographs showed a $CaAl_{12}O_{19}$ layer adjacent to alumina and a $CaAl_4O_7$ layer adjacent to calcium hexaluminate; reacted slag area shows needle like gehlenite crystals, few angular spinel crystals and small amounts of glassy phase.

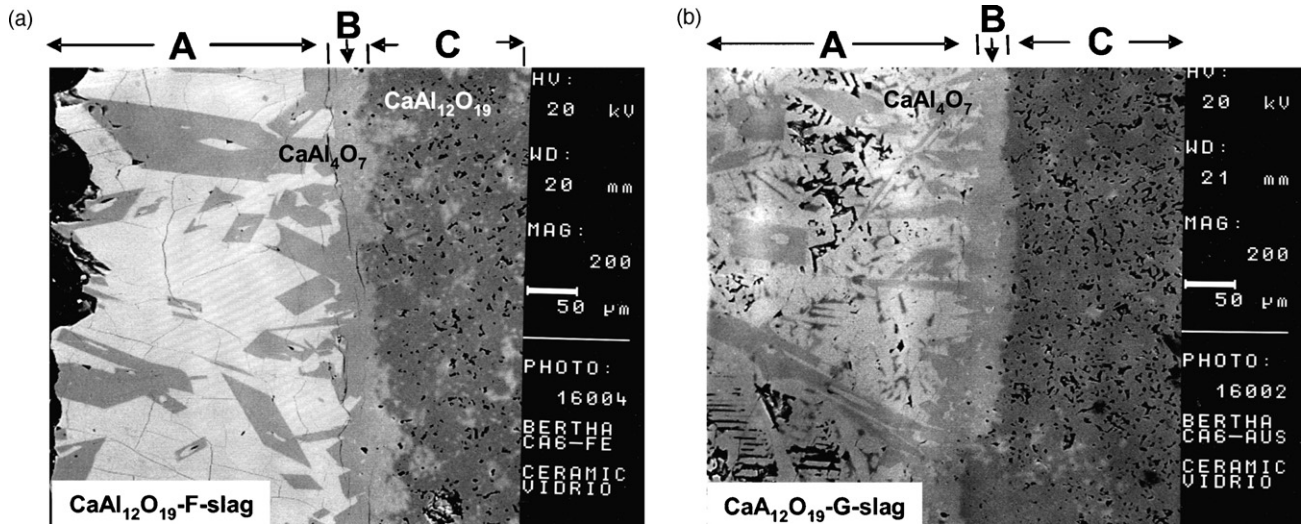

Fig. 7. Higher magnification SEM of: (a) the $CaAl_{12}O_{19}$/F-slag; (b) the $CaAl_{12}O_{19}$/G-slag interfaces. Images show a layer adjacent to hibonite formed by needle like $CaAl_4O_7$ grains and glassy phase.

corundum/F-slag sample. Finally, the thickness and composition of B and C layers was very similar. The region D due to its similitude was not analyzed (Table 3).

The differences found in region A between both samples are again consequence of the different fluidity and melting behaviour of the slags. The higher fluidity of the G-slag enhanced the interaction between the slag and substrate, increased mass transport and consequently the dissolution rate of alumina. The continuous increasing of alumina content in the slag produces the nucleation and growth of the primary gehlenite crystals, while the counter diffusion of Ca^{2+} against Si^{4+} from the slag to substrate (Fig. 6) produces the formation of calcium dialuminate and calcium hexaluminate layers on the substrate interface.

3.3.2. Calcium hexaluminate substrate

SEM micrographs of calcium hexaluminate/F-slag and calcium hexaluminate/G-slag specimens treated at 1578 °C and 1470 °C, respectively, are shown in Fig. 7a and b. It is worth nothing again that the interface sample/slag inside the $CaAl_{12}O_{19}$ substrate is not well defined due to the porosity and microstructural characteristics of the uncorroded hibonite sample. In the mentioned figures the presence of a series of reaction areas formed by reaction between hibonite samples and the corresponding slag is showed (Table 4).

The corrosion behaviour in B and C areas was analogous in both samples. Differences found in region A between both samples were determined by the different viscosity of the slags. An increasing content of CaF_2 into the slag produces a large increase of the dissolution due to a decrease in the slag viscosity.

The microstructure (Fig. 7a and b) of the first reaction area (Region A: ≈280/300 µm) put in evidence the presence of a continuous white and cracked glassy phase and big grey angular primary crystals (20–200 µm) involved in the liquid phase. Energy dispersive X-ray analysis of the mentioned crystals showed an average composition close to $CaAl_2O_4$ (76.9 wt% Al_2O_3 and 23.1 wt% CaO), while the glassy phase, liquid at the reaction temperature, presents an average composition close to gehlenite: (SEM–EDS analysis: 37.8 wt% CaO, 41.0 wt% Al_2O_3 20.1 wt% SiO_2 and 1.1 wt% MgO).

Both effects are consequence of the calcium hexaluminate dissolution into the slag, which produces its enrichment in calcium oxide, and the nucleation and growing of calcium dialuminate crystals. Another effect of the hibonite dissolution is the formation, at the interfaces (B regions), of a thin layer with

Table 3
Mineralogical analyses of every representative area for Al_2O_3/F-slag and alumina/G-slag attack.

Sample	Zone	Thickness (µm)	Mineralogical analysis by SEM–EDS					
			Liquid phase	Gehlenite	$CaAl_4O_7$	$MgAl_2O_4$	$CaAl_{12}O_{19}$	Al_2O_3
Al_2O_3–F-slag	A	0–350	+	+++	+	+	n.d.	n.d.
	B	≈7	+	n.d.	+++	n.d.	n.d.	n.d.
	C	≈15	n.d.	n.d.	n.d.	n.d.	+++	
	D	>3000	n.d.	n.d.	n.d.	n.d.	n.d.	+++
Al_2O_3–G-slag	A	0–560	+++	+	n.d.	n.d.	n.d.	n.d.
	B	≈10	+	n.d.	++	n.d.	n.d.	n.d.
	C	≈20	n.d.	n.d.	n.d.	n.d.	+++	n.d.
	D	n.d.	n.d.	n.d.	n.d.	n.d.	n.d.	+++

n.d.: not detected.

Table 4
Mineralogical analyses of every representative area for $CaAl_{12}O_{19}$/F-slag and $CaAl_{12}O_{19}$/G-slag attack.

Sample	Zone	Thickness (μm)	Mineralogical analysis by SEM–EDS		
			Liquid phase	$CaAl_4O_7$	$CaAl_{12}O_{19}$
$CaAl_{12}O_{19}$–slag F	A	0–280	+++	+	n.d.
	B	≈40	+	+++	n.d.
	C	>300	+	+	+++
	D	>3000	n.d.	+	+++
$CaAl_{12}O_{19}$–slag G	A	0–>300	+++	+	n.d.
	B	≈40	+	+++	n.d.
	C	>300	+	+	+++
	D	>3000	n.d.	+	+++

n.d.: not detected.

a thickness of 40 μm formed by grey and elongated crystals of $CaAl_4O_7$ (SEM–EDS microanalysis 75.5 wt% Al_2O_3, 24.3 wt% CaO), with small quantities of glassy phase at grain boundaries and triple points (Table 4).

Finally as a consequence of the capillarity diffusion of liquid phase through hibonite grain boundaries and pores, a liquid phase sintering process took place in the C region (300 μm), forming a area of increased densification. This low porosity layer and the composition of the reacting liquid, close to the equilibrium, could enhance the corrosion behaviour of the samples. At the bottom of the substrates, behind C, the original porous microstructure of hibonite was observed.

4. Corrosion mechanisms

The results obtained showed that the corrosion processes mainly took place by interaction and penetration of based calcium silicate slags towards the ceramic substrate through grain boundaries in the case of alumina and grain boundaries and open porosity in the case of hibonite material. Interdiffusion and chemical reactions processes between the main components of the liquefied slag Ca, Si, Mg, F and the refractory substrates (Al and Ca) markedly occurred. This fact is supported by the compositional profiles where elements such as Ca, Si, Al, and Mg had significant diffusion patterns (Fig. 5a and b). In both cases, final reaction products were successive layers of calcium aluminates parallel to the front of reaction. A signal corresponding to fluor element was impossible to obtain by SEM/EDS microanalysis.

The saturation solubility of Al_2O_3 and $CaAl_{12}O_{19}$ in both slags has a critical influence on the dissolution process. Although an exact value of the saturation level for alumina and calcium hexaluminate in the present system is not available, various and new phases mainly calcium dialuminate, calcium hexaluminate, and gehlenite were observed. Consequently, the attack of the slag on the substrate is strongly influenced by the composition and thermal behaviour of the slag, composition and microstructure of the substrate and finally by the saturation solubility of the slag.

These effects can be discussed using the involved phase equilibrium diagrams, specifically Al_2O_3–CaO–SiO_2, Al_2O_3–CaO–SiO_2–MgO and Al_2O_3–CaO–SiO_2–CaF_2. Considering that MgO content in both slags are relatively constant and low, around 5 wt%, and that only small amounts of spinel was detected at the alumina–slag interface, the discussion will be made considering the Al_2O_3–CaO–SiO_2–CaF_2 system.

The solid state compatibilities of alumina in this quaternary system (Fig. 8) have been deduced from the corresponding ternary systems found in the literature and the results obtained in the present work. As can be observed in Fig. 8, Al_2O_3, $CaAl_{12}O_{19}$, $Ca_2Al_2SiO_7$ and CaF_2 on one side and $CaAl_{12}O_{19}$, $CaAl_4O_7$, $Ca_2Al_2SiO_7$ and CaF_2 on the other one, are compatible phases. These results are relevant since phase-assemblage in the quaternary system at high temperature are totally similar to those deduced in the Al_2O_3–SiO_2–CaO ternary system since at high temperature CaF_2 is dissolved in the liquid phase and consequently the phases in equilibrium are defined by the Al_2O_3–CaO–SiO_2–liquid or Al_2O_3–CaO–liquid equilibrium. This situation corresponds with the slag/substrate reaction process observed.

Then, the presence of fluorspar in the slags reduces the temperature of first liquid formation and increases the fluidity of the melt, but does not modify the phase assemblage at high temperature. These deductions are in good agreement with the experimental results obtained, which put in evidence: (a) first liquid formation took place at very low temperature; (b) phase-

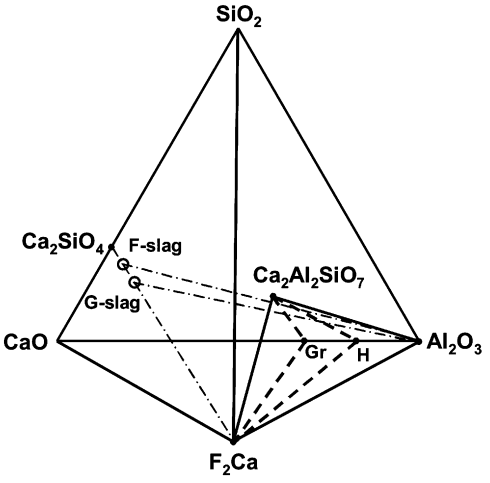

Fig. 8. Sketch of the solid state compatibilities in the Al_2O_3-rich area of the quaternary system Al_2O_3–SiO_2–CaO–F_2Ca. Gr: grosite $CaAl_4O_7$ and H: hybonite $CaAl_{12}O_{19}$. Both slag are also schematically represented.

assemblages observed at high temperature correspond to those defined by the phases involved in the Al_2O_3–CaO–SiO_2–liquid or Al_2O_3–CaO–liquid equilibriums.

4.1. Alumina substrate

In the 1000–1050 °C temperature range a liquid phase sintering of the slags is the predominant process (see Figs. 1 and 2). In this particular case in the temperature interval 1050–1555 °C any significant reaction was observed. The formation of great quantities of liquid phase at corundum–slag interface at $T > 1560$ °C (F-slag) and 1475 °C (G-slag) can be justified by the high and different levels of F_2Ca. The corrosion mechanism can be explained considering the information supplied by the isothermal sections at 1600 °C and 1500 °C of the CaO–Al_2O_3–SiO_2 system (Figs. 9a and 10a, respectively).

Taking into account that the slag compositions are closer to Ca_2SiO_4 or Ca_3SiO_5, the working compositions for the liquid slag,[b] neglecting minor impurities, may be represented by lines going from the calcium disilicate or tricalcium silicate compounds to Al_2O_3. Hence the liquid slag gradually wets and dissolves corundum grains moving its composition along this line. In this process, both slags, after leaving dicalcium or tricalcium silicate + liquid field, consecutively cross the stability fields of liquid and gehlenite + liquid (Figs. 9b and 10b). In both cases, the slag composition evolution justifies the high level of liquid phase found at the interfaces and the crystallization of gehlenite according the following reaction:

$$Ca_2SiO_4/Ca_3SiO_5\ (\text{from slag}) + Al_2O_3\ (\text{from substrate}) \rightarrow Ca_2Al_2SiO_7 \quad (1)$$

In the case of F-slag/alumina sample, after gehlenite formation, the slag composition reaches the $CaAl_4O_7$ + liquid field (L_1 Fig. 10b) where calcium dialuminate starts to crystallize at the slag–oxide interface according to the reaction.[2]

$$CaO\ (\text{from slag}) + 2{\cdot}Al_2O_3\ (\text{from substrate}) \rightarrow CaAl_4O_7 \quad (2)$$

At this point, a $CaAl_4O_7$ layer starts to form due to liquid (slag), which is not in equilibrium with substrate, continues dissolving more alumina and calcium oxide. The process of layer formation ends when the liquid composition, which is moving from L_1 to L_2 (Fig. 10b), reaches the L_2 point.

At this time, when slag reaches the composition defined by the L_2 point, $CaAl_{12}O_{19}$ starts to precipitate according to the reaction.[3]

$$CaAl_4O_7\ (\text{formed at interface}) + 4{\cdot}Al_2O_3\ (\text{from substrate}) \rightarrow CaAl_{12}O_{19} \quad (3)$$

Successive diffusion of Ca-containing liquid phase through the boundaries and pores of the corundum substrate, moves the composition of the slag from L_2 to L_3 (Fig. 10b), which origins a dense and continuous hibonite layer growing from the unreacted corundum substrate. When the slag liquid phase reaches the composition defined by the L_3 point, the liquid composition is in equilibrium, at the same time, with alumina and calcium hexaluminate, thus ending the corrosion process.

On the other hand the small amount of MgO present in the slag reacts with the alumina from the substrate, by a dissolution–precipitation mechanism, forming small amounts of spinel.

$$MgO\ (\text{from slag}) + Al_2O_3\ (\text{from substrate}) \rightarrow MgAl_2O_4 \quad (4)$$

The reactions considered are exothermic and expansive and produced the formation of $MgAl_2O_4$ and $Ca_2Al_2SiO_7$ in the slag and $CaAl_4O_7$ and/or $CaAl_{12}O_{19}$ at the interface.

The corrosion mechanism was similar for alumina/G-slag sample; however the higher quantity of CaF_2 and the elevated basic character of the G-slag, as compared with F-slag, enhances the corrosion process and slightly modifies the attack (Fig. 9a and b).

According the isothermal section at 1500 °C, after gehlenite formation, the line which defines the corrosion process successively intersects the $Ca_2Al_2SiO_7 + CaAl_2O_4 + Liq$ and $Ca_2Al_2SiO_7 + CaAl_2O_4 + CaAl_4O_7$, stability fields. This fact implies: (a) the formation of calcium monoaluminate and the presence of this phase in equilibrium with gehlenite and liquid at the interface; (b) the formation of a solid state area where calcium monoaluminate is in equilibrium with calcium dialuminate and gehlenite. However experimental results, in opposite to theoretical deductions, did not show the presence of the calcium monoaluminate phase neither the phase assemblage mentioned while liquid phase is easily observed. On the other hand, at temperatures lower than 1498 °C, calcium monoaluminate and calcium fluorine react to form $Ca_4Al_6O_{12}F_2$, but this phase melts at 1507 °C and the involved invariant points related to $CaAl_2O_4$ or $Ca_4Al_6O_{12}F_2$ always are lower than 1500 °C.[23]

Then, the differences found between theoretical and experimental results are justified by the high content of F_2Ca in the slag which decreases the temperature of the invariant point of the $CaAl_2O_4$ or $Ca_4Al_6O_{12}F_2$ involved systems and consequently the temperature range at which these phases or related phases assemblage are stable.

At this point of the corrosion process, the composition of the liquid phase defined by the isothermal section corresponds to the L_1 point instead of L*; and consequently $Ca_2Al_2SiO_7 + CaAl_4O_7 + Liq.$, are the stable phase assemblage instead of $Ca_2Al_2SiO_7 + CaAl_2O_4 + Liq.$, in good agreement with the experimental results. The analysis of the section suggest that, liquid is moving its composition from L* to L_1, within the $Ca_2Al_2SiO_7$ + liquid crystallization volume, similarly to the previous one sample.

Afterwards, the corrosion mechanism for this sample exactly follows the same process previously described for the preceding sample.

[b] Liquid is not exactly located on the isothermal section unless on the plane of 10 wt%/15 wt% CaF_2–CaO–SiO_2–Al_2O_3 isothermal sections at 1500 °C and 1600 °C.

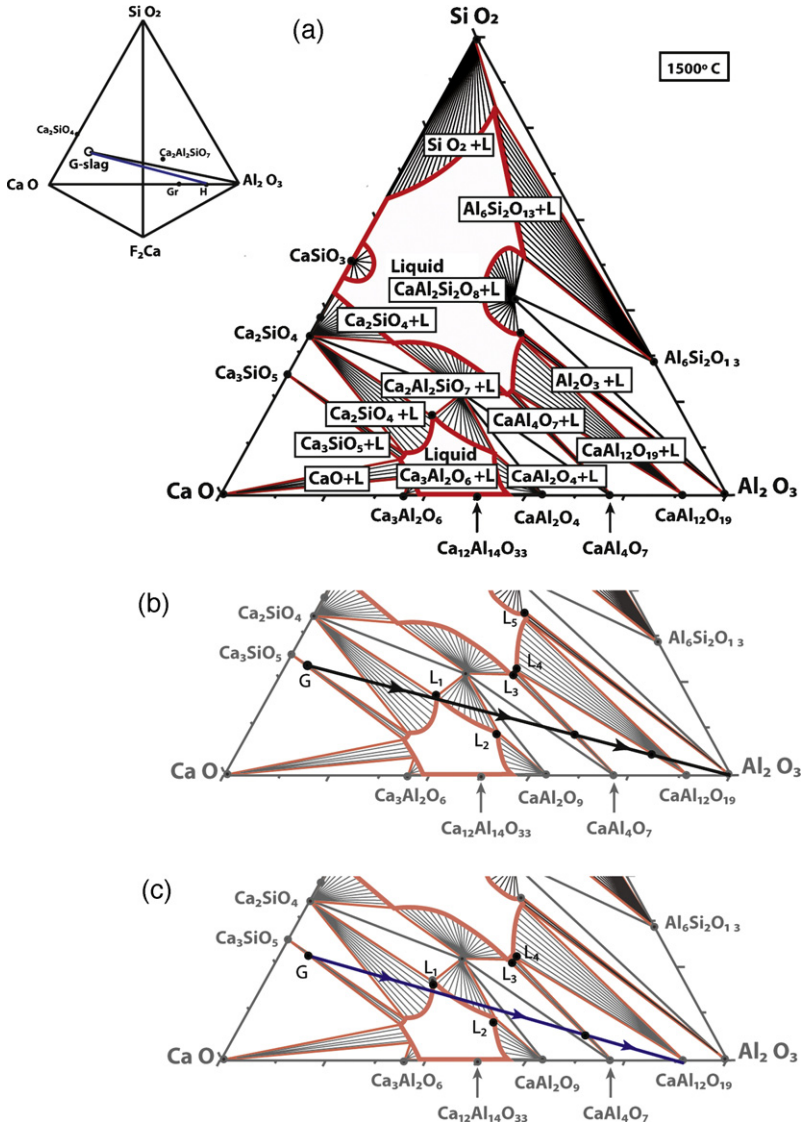

Fig. 9. (a) Isothermal section of Al_2O_3–SiO_2–CaO ternary diagram at 1500 °C; (b) superposed to the isothermal section the sketch of the corrosion process proposed for F-slag–Al_2O_3 interface is showing; (c) superposed to the isothermal section the sketch of the corrosion process proposed for G-slag–$CaAl_{12}O_{19}$ interface is showing.

4.2. Calcium hexaluminate substrate

In this case, in the 1000–1050 °C temperature range, a liquid phase sintering of the slag took place (see Figs. 1 and 2). At higher temperatures, $T > 1400$ °C, the formation of large quantities of liquid phases which enhances reaction mechanism at hibonite–calcium silicate slag interface was observed.

The dissolution of alumina and calcium oxide from $CaAl_{12}O_{19}$ substrate into the slag also causes the liquid composition to move to a composition very close to gehlenite. Considering again the information supplied by the isothermal sections at 1600 °C and 1500 °C of the CaO–Al_2O_3–SiO_2 system (Figs. 9c and 10c), and taking into account slags compositions, the working compositions for the liquid slag corrosion, neglecting minor impurities, may be represented by lines going from the dicalcium silicate (Ca_2SiO_4) or tricalcium silicate (Ca_3SiO_5) crystallization primary field up to $CaAl_{12}O_{19}$, Figs. 9c and 10c for G-slag and F-slag, respectively.

In both samples, the involved mechanism was a dissolution–reaction process. First, calcium hexaluminate crystals were gradually dissolved in the slag which changes its composition along the indicated lines. In this dissolution process the composition of the slag crosses the stability fields of liquid and gehlenite + Liq., which justifies the composition of the liquid phase obtained by SEM–EDS, and the presence of gehlenite at the interface.

In the case of F-slag/$CaAl_{12}O_{19}$, after gehlenite formation, the slag composition reaches the composition defined by L_1 (Fig. 10c) producing the crystallization of calcium dialuminate according to a dissolution–precipitacion reaction.[5]

$$2{\cdot}CaO\ (\text{from slag}) + CaAl_{12}O_{19}\ (\text{from substrate}) \rightarrow 3{\cdot}CaAl_4O_7 \quad (5)$$

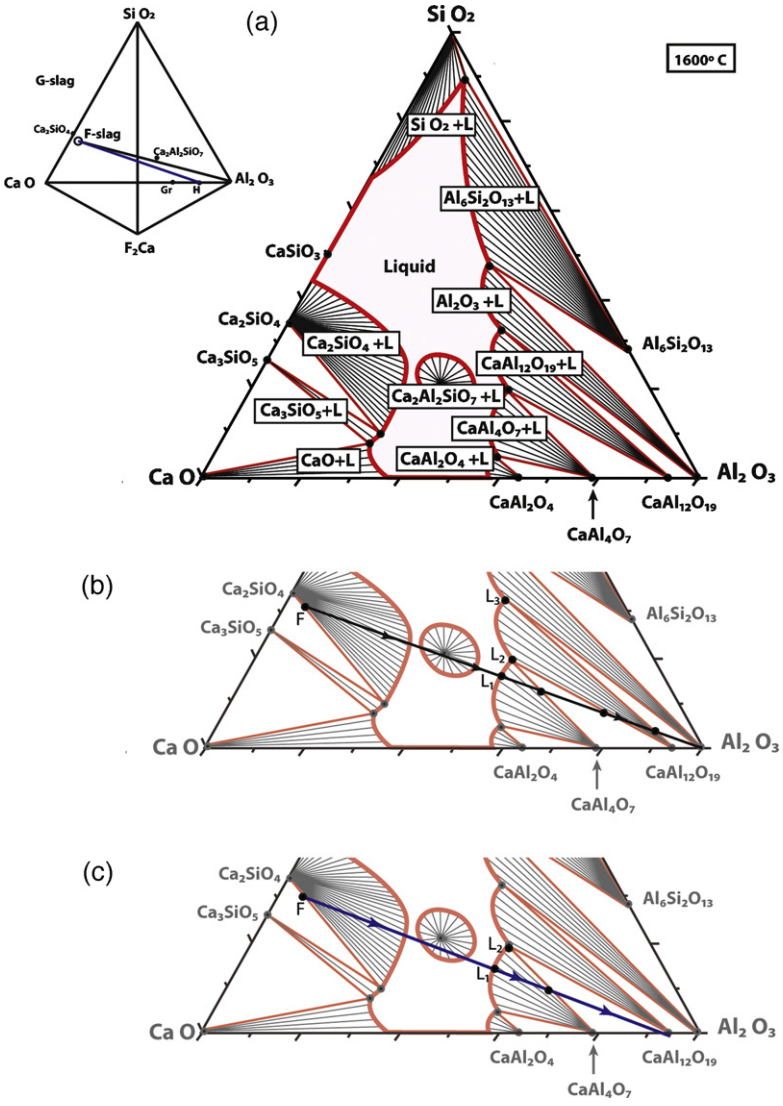

Fig. 10. Isothermal section of Al_2O_3–SiO_2–CaO ternary diagram at 1600 °C; (b) superposed to the isothermal section the sketch of the corrosion process proposed for F-slag–Al_2O_3 interface is showing; (c) superposed to the isothermal section the sketch of the corrosion process proposed for F-slag–$CaAl_{12}O_{19}$ interface is showing.

At this point, a layer of $CaAl_4O_7$ begins to form because the liquid phase (L_1) is not in equilibrium with the substrate and consequently the liquid dissolves more calcium hexaluminate moving its composition along the line L_1–L_2. When the liquid phase composition reaches the L_2 point, the liquid is in equilibrium with calcium dialuminate and calcium hexaluminate at the same time and consequently the corrosion process ends.

The corrosion mechanism in calcium hexaluminate sample against G-slag was very similar as compared with F-slag; however the higher quantity of CaF_2 and the elevated basicity of the G-slag enhance the corrosion process, reducing the temperature of first liquid formation. According the isothermal section at 1500 °C, after gehlenite formation, the line which defines the corrosion process intersects the $Ca_2Al_2SiO_7 + CaAl_2O_4 + Liq$ and $Ca_2Al_2SiO_7 + CaAl_2O_4 + CaAl_4O_7$ stability fields. Again as previous one sample, this fact is associated to the $CaAl_2O_4$ or $Ca_4Al_6O_{12}F_2$ formation, but these phases are not stable at working temperature and not were either detected at the interface. Consequently, differences between theoretical and experimental results are again justified by the high-content of F_2Ca in the slag which, as was mentioned previously, decreases the temperature of the invariant point of the calcium monoaluminate/calcium fluorine involved systems and the temperature range at which this phase or phase assemblage are stable.

Afterwards, the corrosion mechanism for this sample exactly follows the same process previously described for the preceding sample. The liquid moves its composition, within the $Ca_2Al_2SiO_7$ + liquid crystallization volume, from L* to L_1. At L_1 calcium dialuminate starts to precipitate according the reaction (5). The precipitation of this phase, which origins calcium dialuminate layer, continues up to liquid phase reaches the composition defined by L_2, At this point, the corrosion process ends since liquid, calcium dialuminate and calcium hexaluminate are in equilibrium.

5. Conclusions

The corrosion mechanism of alumina and hibonite substrates by calcium silicate-based slags which contain 10 wt% and 15 wt% of fluorspar has been established.

The reaction temperatures between substrates and F-slag/G-slag were established at 1555 and 1430 °C for alumina against F-slag/G-slag and 1555 °C and 1410 °C for hibonite against F-slag and G-slag, respectively.

From microstructural studies, it has been found that corrosion occurs by an interdiffusion mechanism of the liquid slag through grain boundaries in the case of alumina and grain boundaries and porosity in the case of hibonite. Later, reactions by partial dissolution of alumina and hibonite produce the precipitation and the formation of successive layers of calcium dialuminate and calcium hexaluminate at the alumina interface, and a calcium dialuminate layer at the interface in hibonite substrate.

The reaction sequence observed in the alumina substrate such as precipitation of gehlenite, spinel and calcium dialuminate inside the slag region and the formation of calcium dialuminate and calcium hexaluminate successive layers at the alumina interface indicate that indirect or heterogeneous corrosion is the predominant mechanism.

Hibonite substrate also showed precipitation of gehlenite inside the slag region but the dialuminate layer at the interface was not continuous, indicating a dissolution–precipitation process in presence of a liquid phase. Consequently direct or homogeneous corrosion was the predominant mechanism. In this substrate, penetration of the liquid phase via grain boundaries and open pores produced an important sintering and densification process in substrate.

The presence of fluorspar in slag reduces the temperature of first liquid formation and increases the fluidity of the melt enhancing the corrosion process but does not modify both phase assemblages and corrosion mechanisms.

A tentative of the solid state compatibilities of alumina in the quaternary system Al_2O_3–CaO–SiO_2–CaF_2 was established. It was found that phase assemblages at higher temperature (>1500 °C) in presence of liquid phase was similar to those deduced from Al_2O_3–CaO–SiO_2 ternary system. Consequently, the results obtained were discussed taking into account the isothermal section at 1500° and 1600 °C of the Al_2O_3–CaO–SiO_2 system.

Acknowledgements

The authors are indebted to Prof. S. De Aza for important advice and comments during the manuscript writing. We also thank Dr. J.F. Almagro of Acerinox SA for kindly providing calcium silicate slags used in this work. This research was carried out with financial support from MCYT CICYT Projects MAT2006-12749-C02-01 and MAT2007-65857.

References

1. Lee, W. E. and Rainforth, W. M., Refractory materials. *Ceramic-Microstructures-Property Control by Processing*. Chapman and Hall, London, UK, 1994, pp. 470–488.
2. Serena, S., Sainz, M. A. and Caballero, A., Corrosion behaviour of MgO/$CaZrO_3$ refractory matrix by clinker. *J. Eur. Ceram. Soc.*, 2004, **24**, 2399–2406.
3. Pourier, J., Qafssaoui, F., Ildefonse, J. P. and Boucheton, M. L., Análysis and interpretation of refractory microstructures in studies of corrosion mechanisms by liquid oxides. *J. Eur. Ceram. Soc.*, 2008, **28**(8), 1557–1568.
4. Schach, C. A., Corrosion of refractories. In *Refractory Handbook*. Marcel Dekker Inc., New York, 2004.
5. Reed, L. and Barret, L., The slagging of refractories. Part I. The controlling mechanism in refractory corrosion. *Trans. Br. Ceram. Soc.*, 1955, **54**, 671–676.
6. Reed, L. and Barret, L., The slagging of refractories. Part II. The kinetics of corrosion. *Trans. Br. Ceram. Soc.*, 1964, **63**, 509–534.
7. Qafssaoui, F., Poirier, J., Ildefonse, J. P., Hubert, P. and Benyaich, F., Microstructural and physicochemical studies of corroded high alumina refractories. *Silic. Ind. Ceram. Sci. Technol.*, 2005, **70**(7/8), 109–117.
8. Cooper, A. R. and Kingery, W. D., Dissolution in ceramics systems. I. Molecular diffusion, natural convectionand forced convection studies of sapphire dissolution in calcium aluminum silicate. *J. Am. Ceram. Soc.*, 1964, **47**(1), 37–43.
9. Samaddar, B. N., Kingery, W. D. and Cooper Jr., A. R., Dissolution in ceramics systems. II. Dissolution of alumina, mullite, anorthite and silica in a calcium–aluminum silicate slag. *J. Am. Ceram. Soc.*, 1964, **47**(5), 249–254.
10. Oishi, Y., Cooper Jr., A. R. and Kingery, W. D., Dissolution in ceramic systems. III. Boundary layer concentration gradients. *J. Am. Ceram. Soc.*, 1965, **48**(2), 88–95.
11. Sandhage, K. H. and Yurek, G. J., Indirect dissolution of sapphire into silicate melts. *J. Am. Ceram. Soc.*, 1988, **71**(6), 478–489.
12. Sandhage, K. H. and Yurek, G. J., Direct and indirect dissolution of sapphire in calcia–magnesia–alumina–silica melts: dissolution kinetics. *J. Am. Ceram. Soc.*, 1990, **73**(12), 3633–3642.
13. Sandhage, K. H. and Yurek, G. J., Direct and indirect dissolution of sapphire in calcia–magnesia–alumina–silica melts: electron microprobe analysis of the dissolution kinetics. *J. Am. Ceram. Soc.*, 1990, **73**(12), 3633–4442.
14. Guha, J. P., Reaction chemistry in dissolution of polycrystalline alumina in lime–alumina–silica slag. *Br. Ceram. Trans.*, 1997, **96**(6), 231–236.
15. Bates, J. L., Heterogeneous dissolution of refractory oxides in molten calcium–aluminum silicate. *J. Am. Ceram. Soc.*, 1987, **70**(3), C55–C57.
16. Shoichirou, T., Kunihiko, N. and Katsumi, M., Kinetic behaviour of dissolution of sintered alumina into CaO–SiO_2–Al_2O_3. *ISIJ Int.*, 1993, **33**(1), 116–123.
17. Zhang, S., Rezaie, H. R., Sarpoolaky, H. and Lee, W. E., Alumina dissolution into silicate slag. *J. Am. Ceram. Soc.*, 2000, **83**(4), 897–903.
18. Pena, P., Vazquez, B., Caballero, A. and de Aza, S., Quaternary phase equilibrium diagramas. Representation and interpretation method. *Bol. Soc. Esp. Ceram. V.*, 2005, **44**(2), 113–122.
19. Osborn, E. F. and Muan, A., *Phase Equilibria Diagrams of Oxide Systems (Fig. 736)*. The Am. Ceram. Soc. and E. Orton Jr. Ceramic Foundation, 1960.
20. De Vries, R. C. and Osborn, E. F., Phase equilibria in high-alumina part of the system CaO–MgO–Al_2O_3–SiO_2. *J. Am. Ceram. Soc.*, 1957, **40**(1), 6–15.
21. Vázquez, B. A., Caballero, A. and Pena, P., Primary crystallization volume of Al_2O_3 in the quaternary system Al_2O_3–CaO–SiO_2–MgO. *Bol. Soc. Esp. Ceram. V.*, 2004, **43**(1), 16–18.
22. Vazquez, B. A., Caballero, A. and Pena, P., Quaternary system Al_2O_3–CaO–MgO–SiO_2: study of the crystallization volume of $MgAl_2O_4$. *J. Am. Ceram. Soc.*, 2005, **88**(7), 1949–1957.
23. Chatterjee, A. K. and Zhmoiddin, G. I., The system Al_2O_3-CaO-CaF_2. *Inorg. Mater. (USSR) English Translation*, 1972, **8**(5), 769, Taken from Phase Diagrams for Ceramics vol. (5), Fig. 6023. Published by The Am. Ceram. Soc. and E. Orton Jr. Ceramic Foundation (1975).
24. Eitel, W., The system CaO–2CaO·SiO_2–CaF_2. *Zement*, 1938, **27**(31), 469; Eitel, W., *Z. Angew Miner.*, 1938, **1**, 272, Taken from Phase Diagrams for Ceramics vol. (5), Fig. 1708. Published by The Am. Ceram. Soc. and E. Orton Jr. Ceramic Foundation (1975).
25. Gutt, W. and Osborn, G. J., The system CaF_2–CaO–SiO_2. *Trans. Br. Ceram. Soc.*, 1970, **69**(3), 127–128, Taken from Phase Diagrams for Ceramics vol.

(4), Fig. 4882. Published by The Am. Ceram. Soc. and E. Orton Jr. Ceramic Foundation (1975).
26. Gutt, W. and Osborn, G. J., The system CaF_2–$2CaO{\cdot}SiO_2$. *Trans. Br. Ceram. Soc.*, 1966, **65**(9), 529, Taken from Phase Diagrams for Ceramics vol. (3), Fig. 3714. Published by The Am. Ceram. Soc. and E. Orton Jr. Ceramic Foundation (1975).
27. Schlegel, E., The system CaF_2–CaO–MgO. *Z. Chem.*, 1965, **5**(8), 316, Taken from Phase Diagrams for Ceramics vol. (4), Fig. 4881. Published by The Am. Ceram. Soc. and E. Orton Jr. Ceramic Foundation (1975).
28. Hillert, L., The system CaF_2–$5\%Al_2O_3/95\%SiO_2$–SiO_2. *Acta Chem. Scand.*, 1965, **19**(10), 2437, Taken from Phase Diagrams for Ceramics vol. (4), Fig. 4884. Published by The Am. Ceram. Soc. and E. Orton Jr. Ceramic Foundation (1975).
29. Hallstedt, B., Assessment of the CaO–Al_2O_3 system. *J. Am. Ceram. Soc.*, 1990, **73**(1), 15–23.
30. Rodríguez, J. L., de Aza, A. H., Rendón-Ángeles, J. C. and Pena, P., The mechanism of corrosion of MgO–$CaZrO_3$–calcium silicate materials by cement clinker. *J. Eur. Ceram. Soc.*, 2007, **27**, 79–89.
31. Park, J. J. and Min, D. J., Effect of fluorspar and alumina on the viscous flow of calcium silicate melts containing MgO. *J. Non-Cryst. Solids*, 2004, **37**, 150–156.
32. Criado, E., Pena, P. and Caballero, A., Influence of processing method on microstructural and mechanical properties of calcium hexaluminate compacts. *Sci. Ceram.*, 1988, **14**, 193–198.
33. Moya, J. S., de Aza, A. H., Steier, H. P., Requena, J. and Pena, P., Reactive coating on alumina, calcium and barium hexaluminates substrates. *Scripta Metall. et Mater.*, 1994, **31**, 1049–1054.
34. de Aza, A. H., Pena, P. and Moya, J. S., Reactive coating of dolomite on alumina substrates. *J. Eur. Ceram. Soc.*, 1997, **17**(1), 935–941.